

Spin sensitive transport in a spin liquid material: revealing a robustness of spin anisotropy

H. Idzuchi^{1,2,†*}, M. Kimata³, S. Okamoto^{4,5}, P. Laurell⁶, N. Mohanta⁴, M. Cothrine⁷, S. E. Nagler⁸,
D. Mandrus⁷, A. Banerjee^{2,5} and Y. P. Chen^{1,2,5,9,10*}

¹ *WPI Advanced Institute for Materials Research (AIMR)
and Center for Science and Innovation in Spintronics (CSIS), Tohoku University,
Sendai 980-8577, Japan.*

² *Purdue Quantum Science and Engineering Institute and Department of Physics and Astronomy,
Purdue University, West Lafayette, Indiana 47907, USA.*

³ *Institute for Materials Research (IMR), Tohoku University,
Sendai 980-8577, Japan.*

⁴ *Materials Science and Technology Division, Oak Ridge National Laboratory,
Oak Ridge, Tennessee, 37831 USA.*

⁵ *The Quantum Science Center, Oak Ridge National Laboratory, Tennessee, 37831 USA*

⁶ *Computational Sciences and Engineering Division, Oak Ridge National Laboratory,
Oak Ridge, Tennessee 37831, USA.*

⁷ *Department of Materials Science and Engineering, University of Tennessee,
Knoxville, Tennessee 37996, USA.*

⁸ *Neutron Scattering Division, Oak Ridge National Laboratory,
Oak Ridge, Tennessee 37831, USA.*

⁹ *School of Electrical and Computer Engineering and Birck Nanotechnology Center,
Purdue University, West Lafayette, Indiana 47907, USA.*

¹⁰ *Institute of Physics and Astronomy and Villum Centers for Dirac Materials and for Hybrid
Quantum Materials and Devices, Aarhus University, 8000 Aarhus-C, Denmark.*

†Current address: hiroshi.idzuchi@phys.u-tokyo.ac.jp

*Corresponding author. Email: yongchen@purdue.edu

Abstract

Alpha-phase (α -) RuCl_3 has emerged as a prime candidate for a quantum spin liquid (QSL) that promises exotic quasiparticles relevant for fault-tolerant quantum computation. Here, we report spin sensitive transport measurements to probe spin correlation in α - RuCl_3 using a proximal spin Hall metal platinum (Pt). Both transverse and longitudinal resistivities exhibit oscillations as function of the angle between an in-plane magnetic field and the current, akin to previously measured spin Hall magnetoresistance (SMR) in antiferromagnet/Pt heterostructures. The oscillations are observed from 1.5 T to 18 T, both within and beyond the magnetic field range where the antiferromagnetic order and QSL state are reported in α - RuCl_3 . The SMR oscillations show that spins in α - RuCl_3 are largely locked to an in-plane quantization axis transverse to the magnetic field, constituting a continuous-symmetry-broken state that does not necessarily represent a long-range order. This robust anisotropy of spin axis uncovers critical energy scales connected with reported QSL signatures in α - RuCl_3 . Simulations suggest a predominantly antiferromagnetic correlation to moderately high magnetic-fields, that may support the SMR oscillations. The coupling of the spin states within α - RuCl_3 and Pt demonstrated in our experiment opens a transport route to exploring exotic spin phases and device functionalities of QSL materials.

I. INTRODUCTION

Spin liquid material, where spins or magnetic moments do not order down to lowest temperatures, offers exotic quasi-particles and excitations related to electronic spin degree of freedom [1,2]. Lately, alpha-phase (α -) RuCl_3 has attracted significant attention [3,4,5,6] as a promising candidate for the “Kitaev quantum spin liquid (QSL)” that hosts exotic topological gapless and gapped excitations [7]. Alpha-phase RuCl_3 is a strongly spin-orbit-coupled Mott insulator, which has competing bond-dependent nearest-neighbor Kitaev coupling (K_1) as a leading order of exchange couplings, result in quantum frustration despite the absence of geometrical frustration in the honeycomb lattice structure [3]. The phase boundaries in α - RuCl_3 have been characterized by a number of methods including thermodynamic measurements (heat capacity etc. [4,8,9]), static magnetization [10], and neutron scattering [4,11]. It is suggested that the zero-field gapless phase of an ideal Kitaev system can, when subject to a magnetic field in the right direction, turn into gapped phases hosting non-Abelian anyons, which are highly sought after as a means for topological quantum computing [7]. Such gapped QSL states under finite magnetic field [12] have been suggested by nuclear magnetic resonance and neutron scattering measurements in α - RuCl_3 [13,14]. Recent experiments further revealed a quantized thermal transport in the QSL phase under a magnetic field [15-18]. While the moments in zero and low fields partly order in a zigzag antiferromagnetic (AFM) state [11], the nature of the finite-field phase, where the AFM order is supposedly suppressed, including the QSL phase [15,17], remains inconclusive as it is challenging to probe the delicate spin properties when the ordered moments are small or vanishing. In this work, by exploiting spin Hall effects (SHEs [19], in Pt) that couple charge currents with spins, we electrically probe the spin properties of α - RuCl_3 and the dependence on the magnetic field and temperature. In particular, our measurements reveal a broken-symmetry state with established spin quantization axis and spin correlations in a magnetic field and point to distinct energy scales which govern the behaviors of various phases, including the enigmatic QSL phase. Our experimental findings are further corroborated by theoretical calculations of spin correlations.

II. RESULTS

Our experimental technique simply uses a bilayer heterostructure between α -RuCl₃ and platinum (Pt), the most popular nonmagnetic material for SHE to detect spin properties. We employed spin Hall magneto resistance (SMR) technique [20,21] previously studied in a bilayer between Pt and a magnetic insulator. In Pt, a current can generate spin accumulation on the surface (direct SHE: Fig.1(a)), and a spin current can be converted to a charge current (inverse SHE: Fig.1(b)). One can use the spin accumulation induced by Pt to interact magnetically with, and thus characterize, the magnetism in a neighboring material, in this case α -RuCl₃, interfaced with Pt. Backflow of the spin current (from the interface back to Pt) depends on the spin polarization configuration in α -RuCl₃ due to an anisotropic scattering (Figs.1(c) and 1(d)): the spin current prefers to be absorbed when the spins accumulated due to SHE at Pt surface are perpendicular to the magnetic moments in the neighboring insulator (Fig.1C) and reflected when the spins are parallel (or antiparallel) to the moments (Fig.1(d)) [20,24]. In the latter configuration (spins colinear with magnetic moments), the reflected spin current is converted to a charge current additional to the one driven by the external voltage, leading to an increase of longitudinal conductivity in Pt. Such an anisotropic spin-charge conversion at the interface generates an apparent resistivity anisotropy. This means that the electronic transport in Pt becomes dependent on the angle between the magnetic moment direction \hat{X} (vector) in a magnetic insulator and the current direction (Fig.1(c) and 1(d)), making the two longitudinal resistivities ρ_{XX} (current flowing along the magnetic moment direction, Fig.1(c)) and ρ_{YY} (current flowing perpendicular to the magnetic moment direction, Fig.1(d)) unequal (in general $\rho_{XX} > \rho_{YY}$ as explained above and observed previously [24,25], where \hat{Y} is perpendicular to \hat{X}). Upon varying the angle (α) between the direction of the current (thus current induced spin polarization) in the plane relative to the direction of the magnetic moment, oscillations appear for both longitudinal and transverse resistance components (see Supplementary Note 1 for details). This can be conveniently utilized to characterize magnetic properties and spin-dependent phenomena --- even for a magnetic *insulator* with small size --- by transport experiment, using proximal Pt.

We synthesized α -RuCl₃ crystals via vapor transport from pure anhydrous powder (see Appendix A.1 for details). The crystals were cleaved into flakes with the thicknesses of 50 nm (device #1, shown in Fig.1(e)) and 35 nm (device #2). We employed *e*-beam lithography with physical vapor deposition to define Pt Hall bar onto the flakes and the connecting Ti/Au electrodes (including contact pads on the Si substrate). The mean roughness of the flake in device #2 was about 0.03 nm (much less than the thickness of a 2D layer of α -RuCl₃ which is 0.6 nm [4,8]) characterized by atomic force microscopy. The magneto-resistance measurement of α -RuCl₃/Pt Hall bar was performed by changing the strength and the direction of the magnetic field (the electrical probe configuration is shown in (Fig.1(f)). The procedure of the device fabrication and the transport experiment is described in Appendix A.2.

Figure 1(g) shows representative transverse (Hall) and longitudinal resistances as functions of the angle (α , Fig.1(f)) between the magnetic field and the current in plane, measured at a relatively high magnetic field $B = 18$ T. The data show oscillations with an approximate period of π (Fig.1(g)). The oscillations in R_{xy} and R_{xx} are found to have phase-shifts from $\cos 2\alpha$ by $\sim \pi/4$ and $\pi/2$, respectively (the respective dip positions are at $\alpha \sim 45^\circ$ and 0°). We have performed similar measurements on a Pt Hall bar without α -RuCl₃ and did not observe any notable oscillations with a period π (Fig.S2). The oscillation resembles the previous observed SMR for NiO/Pt bilayers, where the Neel vector, or in general the magnetic moments, in NiO (which is an antiferromagnet), are transverse to the magnetic field direction [21,24]. The SMR oscillations in magnet/Pt bilayers have been observed in a number of magnetic insulator materials such as yttrium iron garnet (ferromagnetic (FM)) and NiO (AFM)) [20,24,26]. The longitudinal and transverse resistivity (ρ_{xx} and ρ_{xy}) for an arbitrary direction of in-plane current can be formulated according to previous works [21,24] as

$$\rho_{xx} = \frac{\rho_{xx} + \rho_{yy}}{2} - \frac{\rho_{xx} - \rho_{yy}}{2} \cos 2\alpha, \quad (1)$$

$$\rho_{xy} = -\frac{\rho_{xx} - \rho_{yy}}{2} \sin 2\alpha, \quad (2)$$

for the AFM case, while the oscillation terms would take the opposite (plus) signs for the FM case (see Supplementary Note 1). Additionally, when there is an out-of-plane component of the magnetic field B_z that can appear with a slight misalignment of the field from the sample plane, the ordinary Hall effect (with ordinary Hall resistivity ρ_{Hall}) can give rise to a $\rho_{\text{Hall}}B_z$ term in the transverse resistivity and thus an additional resistance oscillation with a period of 2π (e.g., indicated as $\Delta R_{xy}^{2\pi}$ in Fig.1(g)).

We note that the ground state of α -RuCl₃ at $B = 0$ is believed to be an AFM. It is widely reported that its long-range AFM order is strongly suppressed beyond a critical in-plane field of $B_c = 7 \text{ T} - 8 \text{ T}$ [9-11,27]. At first, this appears at odds with our observation of AFM-like SMR (Fig.1(g)) at much higher fields such as $B = 18 \text{ T}$ where there is presumably no longer a long-range AFM order. However, we point out here that the anisotropic transport nature underlying the SMR actually does *not* necessarily require a long-range magnetic order: one can have a SMR (and associated angular oscillation) as long as a preferred spin quantization axis $\pm \hat{X}$ (note $-\hat{X}$ is in the same axis as $+\hat{X}$) is present. Figure 1(h) shows an example for a honeycomb lattice with spins (polarization direction \hat{S}), without any apparent magnetic (FM or AFM) long-range order, yet all the lattice spin have chosen a quantization axis $\pm \hat{X}$ nearly perpendicular to the applied field (with axis \hat{B}), that can generate AFM-like SMR as

$$\hat{S} // \pm \hat{X}, \quad \angle(\hat{S}, \hat{B}) \approx \pm \pi/2. \quad (3)$$

This means neither a magnetic order nor, more generally, a static magnetic superlattice are needed to generate the SMR and associated resistance oscillations. It can be viewed as an analogue of spin-flop state but covers more general spin configuration that does not require a long-range magnetic order. It is also worth mentioning that the contribution to SMR may not change even if spin direction reverses the sign (such as between $\pm \hat{X}$). We propose that for an AFM material, the Zeeman energy can make it energetically favorable for the spins to be perpendicular to the field, even without any apparent AFM order (assuming the energy scale of the spin anisotropy within the plane is not too strong compared to the Zeeman energy). The spontaneous choice in quantization axis at low temperature can also be inferred from the “equal-time” spin correlation (as explained later in our theoretical simulations producing consistent spin configurations). Our experimentally observed, well-defined SMR oscillation suggests that the long-range spin correlation (in the sense that the spins across the sample have chosen one quantization axis direction, without necessarily a static long-range spin order) has a length scale over $10 \mu\text{m}$ (the size of our sample).

The magnetic field dependence of the SMR signal (angular oscillation) for device #1 is shown in Fig.2(a) (representative traces) and Fig.2(b) (plotted in interpolated color scale, with all traces shown in Fig.S3). The SMR data were fitted to characterize the amplitude and the phase of the oscillations with $\Delta R_{xy}^{\pi} \cos(2(\alpha - \alpha_{\text{SMR}}) + \pi) + \Delta R_{xy}^{2\pi} \cos(\alpha + A) + B + C\alpha$ where ΔR_{xy}^{π} , α_{SMR} , $\Delta R_{xy}^{2\pi}$, A , B (the offset), and C (the linear drift slope) are free fitting parameters (see Supplementary Note 2 for details). We observed an AFM-like phase (phase shift by $\sim 45^\circ$ from $\cos 2\alpha$) over the entire range of fields studied (0 T to 18 T). On the other hand, the amplitude grows rapidly with the field up to about $B_c \sim 7 \text{ T}$, and above it the amplitude no longer increases appreciably and rather saturates (Fig.2(c)). This result suggests that the spin correlation (an AFM-like quantization axis transverse to magnetic field developed across the sample) responsible for the SMR is still dominant even above B_c . As we argue below, our results are not in antithesis to the suppression of static long-range AFM order in α -RuCl₃ beyond $B_c \sim 7 \text{ T}$ based on early studies [9-11,17,27,28]. It requires us to consider a more general SMR scenario instead of the special case of the previously studied SMR with long-range spin order.

The spin correlations signify the establishment of a quantization axis associated with an order parameter and an energy scale. In order to explore such energy scales, the temperature dependence of the SMR is measured in α -RuCl₃/Pt. An overarching feature is that the SMR oscillation amplitude rapidly decreases with increasing temperature until becoming difficult to discern given the noise level of the measurement (Figs.3(a) and 3(c), the oscillation phases are shown in Figs.3(b) and 3(d)). This feature is pronounced below B_C where a linear fit to the temperature-dependent amplitude on the low temperature side (blue region in Fig.3(a)) shows the zero-amplitude intercepts at $T = 6.6 \pm 0.5$ K for $B = 5.0$ T and $T = 8.2 \pm 0.5$ K for $B = 4.0$ T (overall average of $T_C = 7.9$ K, over four fitted lines for 4.0, 5.0, 7.5, and 8.0 T in Fig.3(a)). The absence of SMR at low magnetic fields above those temperatures implies the relevant anisotropic spin correlations are suppressed significantly, or there may exist similar amounts of spin correlations with quantization axes parallel and perpendicular to the magnetic field leading to no net observable SMR oscillations. We can note here that this temperature scale, T_C , is consistent with the range of Néel temperatures (with $T_{C0} \approx 7$ -7.5K at zero field [8,15,18]) reported for α -RuCl₃ for the phase transition from an AFM long-range-ordered state at low temperature to a Kitaev paramagnet at high temperature, as probed by other techniques on bulk samples. However, what is notable is that even data at fields of 7.5 T and beyond (above B_C) still exhibit the similarly rapid suppression of SMR with temperature (blue shaded region), beyond which the SMR decays more slowly but remains observable for higher temperature, indicating the persistence of the spin correlations beyond B_C , practically all the way to 14.5 T with essentially the same characteristic energy scale T_C (zero-amplitude intercept of the blue hypotenuse region in Fig.3(a)). Importantly, T_C is on the similar order of the temperature scales to which the quantized thermal Hall effect in transverse thermal conductivity κ_{xy} (6.5 K in [18]), or the Shubnikov-de-Haas like oscillations in longitudinal κ_{xx} (~ 4 K in [16]), have been previously observed in α -RuCl₃. Our results are suggestive of a correlation phenomenon (possibly pertaining to in-plane antiferromagnetic fluctuation discussed below) unassociated with long-range order, but with a well-defined quantization axis with a single energy scale of $T_C \sim 8$ K, seemingly responsible for both long-range order at low fields and exotic quantum states at higher fields.

At higher magnetic fields, the SMR signal amplitude decays more slowly but does not fully reduce to zero (Fig.3(a), green region) even at temperatures significantly above T_{C0} . This may indicate the existence of a second, yet higher energy scale, that also plays a role for the ordering and correlation relevant for SMR. Further characteristics above T_{C0} , for example at 8 K and 12 K (Fig.3(c)), reveal that even if the SMR is unobservable at low fields, it can reappear with increasing field. This indicates the strong magnetic field can induce strong spin-correlation in α -RuCl₃ while suppressing the AFM long-range order. Despite usual expectations that a high field should polarize the system into a ferromagnet-like order, we observe in our SMR measurement a state that is more *antiferromagnet*-like (in terms of spin correlation, even without AFM order). This result is counter-intuitive and argues against the ~ 14 T state to be connected to a fully polarized state, and addresses why the saturation magnetic field in α -RuCl₃ is indeed very high (reported to be ~ 60 T, [10]). It will be an interesting future investigation to explore the full energetics of the green region in Fig.3(a) and its relation to scale-invariant critical behavior to very high field and temperature scales [29].

III. SIMULATION

We have simulated the spin correlations in α -RuCl₃ using a minimal 2D model with J_1 - K_1 - Γ_1 - Γ_1' - J_3 terms following many previous works [9-11, 15, 17, 27, 30-35 and some other relevant literatures are listed in [30, 31]), where J_1 (J_3) is the first (third) nearest neighbor (NN) Heisenberg term, Γ_1 is the symmetric off-diagonal interaction term, and Γ_1' is the symmetric off-diagonal interaction term originating from trigonal distortion (see Appendix A.3 for details). Our classical Monte Carlo (MC) simulation was performed at the default temperature of $T = 2$ K unless otherwise

specified. Based on the parameters in [32] (Appendix A.3), our classical MC simulation shows an AFM transition temperature of ~ 6 K (extracted from the temperature dependence of spin correlation, Fig.S6), which is close to the T_{C0} values in experimental reports [10,27,34]. Importantly, the instantaneous (equal-time) spin correlation function (Fig.4(a), for field along b axis) shows a notable zigzag AFM correlation at wavevector M_3 , where M_3 represents a magnetic superlattice with a period of one atom in the b direction whereas the spin quantization axis is in the a direction. The correlation (reflected in $\langle S_{-M_3}^a S_{M_3}^a \rangle$, where $\langle S_{-\mathbf{k}}^\eta S_{\mathbf{k}}^\eta \rangle$ is a statistical average of $S_{-\mathbf{k}}^\eta S_{\mathbf{k}}^\eta$, \mathbf{k} is the momentum and $\eta = a, b$) slowly decreases above $B \sim 8$ T but survives up to rather high fields far above $B_C \sim 7$ T. When computed with the exact diagonalization method (at zero temperature) where the quantum effects on magnetic properties are fully included (note classical MC simulations do not capture the quantum fluctuations), the AFM correlation at wavevector M_3 , $\langle S_{-M_3}^a S_{M_3}^a \rangle$, is more robust against the magnetic field (see Supplementary Note 3 and Fig.S7), indicating the importance of quantum fluctuations in the field-induced AFM correlation.

This feature is also seen in the real-space snapshots of α -RuCl₃ spin configuration shown in Figs.4(b)-4(e). In the wide magnetic field-range from 0 T to 15 T, a clear AFM structure in a single snapshot appears in real-space, manifesting a robust AFM correlation (Figs.4(b)-4(e)). With a field direction along b , i.e. along a Ru-Ru bond (Z bond direction, see Fig.S5(b) for clarifications of the directions), a zigzag pattern appears, exhibiting prominent spin component (S^a) along a (transverse to b direction) with the sign (shown as red and blue in Figs.4(b)-4(e)) alternating along b between neighboring zigzag chains. Note in general the sixfold symmetry can yield three degenerated zigzag patterns alternating along X, Y, Z bond directions (inset of Fig.4(b)) at zero field (where the system likely containing domains of the three directions, while one type of domains, along the Z, likely become favored when increasing the magnetic field along Z, see Supplementary Note 4). Strikingly, the AFM zigzag structure is seen and survives even above the critical field B_C [11,27] where the long-range AFM order is suppressed. In other in-plane field directions (such as $B \parallel a$), it is reported that AFM long-range order is similarly suppressed beyond 7 T – 8 T [36]. The spin correlation with the magnetic field along other directions were similarly computed and does not qualitatively change our conclusion. This includes the case for $B \parallel a$ where the Chern number in the Kitaev model is expected to be ± 1 [17]. Note our simulation shows a growing FM correlation component $\langle S_{-\Gamma}^b S_{\Gamma}^b \rangle$, which overcomes the AFM correlation component $\langle S_{-M_3}^a S_{M_3}^a \rangle$, at very high field. This however may not make a significant difference for SMR due to strong spin fluctuation at low energy (see Supplementary Note 3 for detail). Extension to 3D Hamiltonian may also suppress the FM-like contribution (see Supplementary Note 4 for detail).

IV. DISCUSSION

The existence of the spin correlation at elevated temperatures observed in our experiment can be further corroborated by simulations, performed for the a -component of spin with and without an external magnetic field applied in b -axis, at $T = 10$ K (Fig.5). Without the magnetic field, we find no noticeable spin correlation beyond fluctuation (Fig.5(a)), as expected from the energy difference between competing AFM and FM states reported to be ~ 10 K [37]. With increasing in-plane field, the zigzag AFM correlation is more pronounced and the relevant spin unit vectors are gradually forced to align perpendicularly to the field direction, reaching significant transverse spin component at $B = 15$ T (Figs.5(b)-5(d)). The experiment and simulation both suggesting transverse spin correlation at elevated temperatures with high fields are in contrast with arguments [38,39] of the development of ferromagnetic correlations, a partial polarized phase, or a conventional paramagnet to fields above 18 T. Magnetic anisotropies in α -RuCl₃ and its microscopic origin are discussed in Supplementary Note 4.

Both the magnetic field and temperature anomalies seen in the SMR experiment (Figs. 2 and 3) correlate with the reported values for the transition to the phase in which quantization and oscillation of thermal transport are reported (although in different experiments [15-18]): e.g., ~ 7 T

and ~ 9.5 T (Figs.2(c) and 3(c): where the SMR amplitude shows kinks) at 2 K, and ~ 8 K (Fig.3(a): where the SMR amplitudes go down to zero) at 7.5 T and 8 T. Also, anomalies appear around 10 T in the field dependence, as SMR at high temperature start to appear (Fig.3(c)) and SMR phase stop to decrease (Fig.3(d)) above this field. This is the field where the soft anomalies have been observed in magnetorestriction [39] and longitudinal thermal transport [18], where magnon-like features reappear in Raman spectroscopy [40,41] and where the Shubnikov-de-Haas like oscillations in κ_{xx} subside [16]. Importantly, our experiment indicates the single energy scale of ~ 8 K, in striking corroboration of recent characterizations of the QSL that have revealed an energy scale in the range form ~ 5 K to ~ 9 K, both by longitudinal and transverse (Hall) thermal transport measurements [15-18, 42] as well as heat capacity [42] studies. Our SMR techniques have provided a highly sensitive probe to examine spin correlations and quantization axes revealing a continuous symmetry broken phase in an in-plane field (Fig.1(h)), which are complementary to the ordering revealed by bulk reciprocal-space techniques such as Raman and neutron scattering. This provides important physical input to identify microscopic origin of the energy scale, including a scenario of spinon excitation in the Fermi surface in the QSL state [16, 43], where a broken continuous symmetry is present.

There have been few spin-sensitive electrical probes that can be adopted to characterize the finite-field phase of an exotic magnet, including spin liquid with higher dimensions than one [44], like α -RuCl₃. Our approaches allow using electric transport to probe insulating materials (even for samples of small dimensions and in the atomically thin limit, which allows to study dimensional crossover and interlayer coupling) and their quasi-particle excitations, including to probe the correlation between spins that can be fluctuating and need not be ordered. Our method can be further combined with or adapted to other experimental techniques such as scanning probe microscopies, and high-frequency transport in similar heterostructures and is complementary to the reciprocal-space techniques such as Raman and neutron scattering. The study is also an example applying spintronic techniques to study quantum materials and explore novel phases of matter.

ACKNOWLEDGMENTS

We thank Q. Niu, D. Xiao and G. Bauer for helpful discussions. This work was supported in part by AIMR and its “fusion” research program, under World Premier International Research Center Initiative (WPI), the Ministry of Education, Culture, Sports, Science and Technology (MEXT), Japan, and by Grant-in-Aid for Scientific Research, JSPS KAKENHI (Grant Numbers 20K14399, 18H03858 and 19K03736), by Center for Science and Innovation in Spintronics, by GIMRT Program (High Field Laboratory for Superconducting Materials) of the Institute for Materials Research, and by Center for Integrated NanoTechnology Support, Tohoku University. The research by S.O. and P.L. was supported by the Scientific Discovery through Advanced Computing (SciDAC) program funded by the US Department of Energy (DOE), Office of Science, Advanced Scientific Computing Research. N.M. was supported by the DOE, Office of Science, Basic Energy Sciences, Materials Sciences and Engineering Division. M.C., S.E.N., and D.M. acknowledge support from National Science Foundation (NSF grant number DMR-1808964). S.O. (later stage of his research), A.B. and Y.P.C. also acknowledge support by Quantum Science Center (QSC), a US DOE National Quantum Information Science Research Center. This research used resources of the Oak Ridge Leadership Computing Facility, which is a DOE Office of Science User Facility supported under Contract DE-AC05-00OR22725, and of the Compute and Data Environment for Science (CADES) at the Oak Ridge National Laboratory, which is managed by UT-Battelle and supported by the Office of Science of the U.S. DOE under Contract No. DE-AC05-00OR22725.

APPENDIX A: MATERIALS AND METHODS

1. Crystal synthesis

Single-crystal RuCl_3 was synthesized via chemical vapor transport from pure anhydrous powder. Commercial $\alpha\text{-RuCl}_3$ powder was sealed under vacuum in a quartz ampoule and heated to $1060\text{ }^\circ\text{C}$ at a rate of $1.6\text{ }^\circ\text{C}/\text{min}$. The ampoule was held at this temperature for 12 hours before being cooled to $600\text{ }^\circ\text{C}$ at a rate of $6\text{ }^\circ\text{C}/\text{hr}$, at which point the growth was allowed for furnace cool back to room temperature. The crystals grew as shiny black plates, typically around $0.5\text{ cm} \times 0.5\text{ cm}$ in lateral size and around 0.5 mm in thickness, though some larger crystals were also obtained. Samples were characterized by X-ray diffraction to determine phase purity. Samples were then characterized by magnetic susceptibility measurements. All the crystals were measured and a single peak in the susceptibility was observed at approximately 7.85 K (Fig.S4), which has been shown to be evidence of low stacking fault density [8].

2. Procedure of Device fabrication and transport experiment

The $\alpha\text{-RuCl}_3$ flakes were mechanically cleaved from the crystals on silicon substrate (Si with 285-nm-thick SiO_2). For device #1, the standard e -beam lithography process was applied to pattern the platinum Hall bar, titanium/gold (depositing 5-nm-thick Ti on SiO_2 to improve the adhesion followed by 60-nm-thick Au) electrical leads and pads. The optical micrograph of the device is shown in Fig.1(e) (device #1). For device #2, we first prepared a 3-nm-thick Pt film on silicon substrate and then $\alpha\text{-RuCl}_3$ was mechanically cleaved on Pt film. After the Au pads are formed on Pt (at the areas without the $\alpha\text{-RuCl}_3$ flake), the $\alpha\text{-RuCl}_3/\text{Pt}$ bilayer is patterned to Hall bar by e -beam lithography and Ar ion-milling. The thicknesses and the roughness were characterized by atomic force microscopy. The thicknesses of the $\alpha\text{-RuCl}_3$ flakes were 50 nm for device #1 and 35 nm for device #2. The mean roughness of the flake for the device #2 was about 0.03 nm. The $\alpha\text{-RuCl}_3$ flakes were characterized by Raman microscopy after e -beam process, and did not show noticeable degradation. The magneto resistance measurement of Pt/ $\alpha\text{-RuCl}_3$ Hall bar was performed (the electrical probe configuration is shown in Fig.1(f)) in a cryostat with superconducting magnet and a two-axis sample rotation probe. The rotation plane is carefully calibrated using a Hall sensor and the perpendicular component of the field is minimized.

3. Theoretical approach

In the simulation, we employed the following Hamiltonian with $J_1\text{-}K_1\text{-}\Gamma_1\text{-}\Gamma_1'\text{-}J_3$ terms

$$\begin{aligned} \mathcal{H}_{J_1-K_1-\Gamma_1-\Gamma_1'-J_3} &= \sum_{\langle i,j \rangle} \left[J_1 \mathbf{S}_i \cdot \mathbf{S}_j + K_1 S_i^X S_j^X + \Gamma_1 (S_i^X S_j^Y + S_i^Y S_j^X) + \Gamma_1' \sum_{\alpha \neq \gamma} (S_i^\alpha S_j^\gamma + S_i^\gamma S_j^\alpha) \right] \\ &+ J_3 \sum_{\langle\langle i,j \rangle\rangle} \mathbf{S}_i \cdot \mathbf{S}_j, \end{aligned}$$

where $\langle \dots \rangle$ and $\langle\langle \dots \rangle\rangle$ denote nearest-neighbor (NN) sites and third-nearest-neighbors (3NN) sites, \mathbf{S}_i is a spin with $S=1/2$ interacting via the NN (3NN) Heisenberg exchange $J_{1(3)}$, the bond-dependent Kitaev interaction K_1 , and symmetric off-diagonal interactions Γ_1 and Γ_1' . The bond dependence of the Kitaev term is indicated by X, Y, Z (its direction is presented in Figs.4(b) and S5(b)) for a given combination of spin site (i, j) , which determines γ as $x, y, \text{ or } z$ respectively, and α, β are other two spin components. This Hamiltonian has been widely used to study the magnetic properties of Kitaev compounds on the honeycomb lattice. For our analysis, we mainly use the parameter set of the modified ab initio model [32]: $J_1 = -1.3\text{ meV}$, $K_1 = -15.1\text{ meV}$, $\Gamma_1 = 10.1\text{ meV}$, $\Gamma_1' = -0.1175\text{ meV}$, $J_3 = 0.9\text{ meV}$ (K_2 and K_3 , second-nearest-neighbors and 3NN analogs to K_1 , are neglected for simplicity). This model is analyzed using the Lanczos exact diagonalization (ED) method, as well as a Monte Carlo (MC) simulation with the Metropolis algorithm by approximating quantum spins as classical vectors. Because the size of the Hamiltonian matrix grows exponentially with respect to the system size, ED uses C_3 -rotationally invariant 24-site clusters respecting the

lattice symmetry. On the other hand, MC can handle much larger system sizes, and for the main results presented here we use 7200-site clusters. In both cases, we impose periodic boundary conditions. To study momentum dependent equal-time spin-spin correlation functions with MC, the 1st BZ is divided into 12 patches (which are available for the 24-site cluster used in ED), and the correlation functions are averaged in each patch to allow direct comparison with the ED results (see supplementary information, Fig.S5). The effect of an applied magnetic field in the ab plane is studied by using the g factor $g_{ab} = 2.3$. Note that the crystal axes $\{a, b, c\}$ and the local spin axes $\{x, y, z\}$ are different (c is an axis perpendicular to ab plane). In the current setup, the Z bonds of the Kitaev interaction are taken parallel to the crystallographic b axis, and the spin z component S^z is taken along one of the Ru-Cl bonds, that is perpendicular to the b axis [45], as shown in Fig.S5B. Thus, $\{S^x, S^y, S^z\}$ and $\{S^a, S^b, S^c\}$ are related by the following 3×3 matrix:

$$\begin{bmatrix} S^x \\ S^y \\ S^z \end{bmatrix} = \frac{1}{\sqrt{6}} \begin{bmatrix} 1 & -\sqrt{3} & \sqrt{2} \\ 1 & \sqrt{3} & \sqrt{2} \\ -2 & 0 & \sqrt{2} \end{bmatrix} \begin{bmatrix} S^a \\ S^b \\ S^c \end{bmatrix}.$$

REFERENCES

- [1] P. W. Anderson, Resonating valence bonds: a new kind of insulator? *Mater. Res. Bull.* **8**, 153–160 (1973).
- [2] L. Savary & L. Balents, Quantum spin liquids: a review. *Rep. Prog. Phys.* **80**, 016502 (2016).
- [3] H.-S. Kim, V. S. V. A. Catuneanu, H.-Y. Kee, Kitaev magnetism in honeycomb α - RuCl_3 with intermediate spin-orbit coupling. *Phys. Rev. B* **91**, 241110 (2015).
- [4] A. Banerjee, C. A. Bridges, J. Q. Yan, A. A. Aczel, L. Li, M. B. Stone, G. E. Granroth, M. D. Lumsden, Y. Yiu, J. Knolle, S. Bhattacharjee, D. L. Kovrizhin, R. Moessner, D. A. Tennant, D. G. Mandrus, S. E. Nagler, Proximate Kitaev quantum spin liquid behaviour in a honeycomb magnet. *Nat. Mater.* **15**, 733-740 (2016).
- [5] L. J. Sandilands, Y. Tian, K. W. Plumb, Y. J. Kim, K. S. Burch. Scattering continuum and possible fractionalized excitations in α - RuCl_3 . *Phys. Rev. Lett.* **114**, 147201 (2015).
- [6] J. Nasu, J. Knolle, D. L. Kovrizhin, Y. Motome, R. Moessner. Fermionic response from fractionalization in an insulating two-dimensional magnet. *Nat. Phys.* **12**, 912 (2016).
- [7] A. Kitaev, Anyons in an exactly solved model and beyond. *Ann. Phys.* **321**, 2-111 (2006).
- [8] H. B. Cao, A. Banerjee, J. Q. Yan, C. A. Bridges, M. D. Lumsden, D. G. Mandrus, D. A. Tennant, B. C. Chakoumakos, S. E. Nagler, Low-temperature crystal and magnetic structure of α - RuCl_3 . *Phys. Rev. B* **93**, 134423 (2016).
- [9] I. A. Leahy, C. A. Pocs, P. E. Siegfried, D. Graf, S. H. Do, K.-Y. Choi, B. Normand, M. Lee, Anomalous Thermal Conductivity and Magnetic Torque Response in the Honeycomb Magnet α - RuCl_3 . *Phys. Rev. Lett.* **118**, 187203 (2017).
- [10] Y. Kubota, H. Tanaka, T. Ono, Y. Narumi, K. Kindo, Successive magnetic phase transitions in α - RuCl_3 : XY-like frustrated magnet on the honeycomb lattice. *Phys. Rev. B.* **91**, 094422 (2015).
- [11] J. A. Sears, Y. Zhao, Z. Xu, J. W. Lynn, Y.-J. Kim, Phase diagram of α - RuCl_3 in an in-plane magnetic field. *Phys. Rev. B* **95**, 180411 (2017).
- [12] Z.-X. Liu, B. Normand, Dirac and Chiral Quantum Spin Liquids on the Honeycomb Lattice in a Magnetic Field. *Phys. Rev. Lett.* **120**, 187201 (2018).
- [13] A. Banerjee, P. Lampen-Kelley, J. Knolle, C. Balz, A. A. Aczel, B. Winn, Y. Liu, D. Pajerowski, J. Yan, C. A. Bridges, A. T. Savici, B. C. Chakoumakos, M. D. Lumsden, D. A. Tennant, R. Moessner, D. G. Mandrus, S. E. Nagler, Excitations in the field-induced quantum spin liquid state of α - RuCl_3 . *npj Quantum Materials* **3**, 8 (2018).
- [14] N. Janša, A. Zorko, M. Gomilšek, M. Pregelj, K. W. Krämer, D. Biner, A. Biffin, C. Rüegg, M. Klanjšek. Observation of two types of fractional excitation in the Kitaev honeycomb magnet. *Nat. Phys.* **14**, 786 (2018).
- [15] Y. Kasahara, T. Ohnishi, Y. Mizukami, O. Tanaka, S. Ma, K. Sugii, N. Kurita, H. Tanaka, J. Nasu, Y. Motome, T. Shibauchi, Y. Matsuda. Majorana quantization and half-integer thermal quantum Hall effect in a Kitaev spin liquid. *Nature* **559**, 227-231 (2018).
- [16] P. Czajka, T. Gao, M. Hirschberger, P. Lampen-Kelley, A. Banerjee, J. Yan, D. G. Mandrus, S. E. Nagler, N. P. Ong. Oscillations of the thermal conductivity in the spin-liquid state of α - RuCl_3 . *Nat. Phys.* **17**, 915 (2021).
- [17] T. Yokoi, S. Ma, Y. Kasahara, S. Kasahara, T. Shibauchi, N. Kurita, H. Tanaka, J. Nasu, Y. Motome, C. Hickey, S. Trebst, Y. Matsuda. Half-integer quantized anomalous thermal Hall effect in the Kitaev material α - RuCl_3 . *Science* **373**, 568-572 (2021).
- [18] J.A.N. Bruin, R.R. Claus, Y. Matsumoto, N. Kurita, H. Tanaka, H. Takagi. Robustness of the thermal Hall effect close to half-quantization in a field-induced spin liquid state. *arXiv preprint arXiv:2104.12184* (2021).
- [19] J. Sinova, S. O. Valenzuela, J. Wunderlich, C. H. Back, T. Jungwirth, Spin Hall effects. *Rev. Mod. Phys.* **87**, 1213-1260 (2015).
- [20] H. Nakayama, M. Althammer, Y. T. Chen, K. Uchida, Y. Kajiwara, D. Kikuchi, T. Ohtani, S. Geprägs, M. Opel, S. Takahashi, R. Gross, G. E. W. Bauer, S. T. B. Goennenwein, E. Saitoh, Spin Hall Magnetoresistance Induced by a Nonequilibrium Proximity Effect. *Phys. Rev. Lett.* **110**, 206601 (2013).
- [21] Y.-T. Chen, S. Takahashi, H. Nakayama, M. Althammer, S. T. B. Goennenwein, E. Saitoh, G. E. W. Bauer, Theory of Spin Hall Magnetoresistance. *Phys. Rev. B* **87**, 144411 (2013).

- [22] A. Kovalev, A. Brataas, G. Bauer, Spin transfer in diffusive ferromagnet--normal metal systems with spin-flip scattering. *Phys. Rev. B* **66**, 224424 (2002).
- [23] H. Idzuchi, Y. Fukuma, S. Takahashi, S. Maekawa, Y. Otani, Effect of anisotropic spin absorption on the Hanle effect in lateral spin valves. *Phys. Rev. B* **89**, 081308 (2014).
- [24] G. R. Hoogeboom, A. Aqeel, T. Kuschel, T. T. M. Palstra, B. J. van Wees, Negative spin Hall magnetoresistance of Pt on the bulk easy-plane antiferromagnet NiO. *Appl. Phys. Lett.* **111**, 052409 (2017).
- [25] K. Ganzhorn, J. Barker, R. Schlitz, B. A. Piot, K. Ollefs, F. Guillou, F. Wilhelm, A. Rogalev, M. Opel, M. Althammer, S. Geprägs, H. Huebl, R. Gross, G. E. W. Bauer, S. T. B. Goennenwein, Spin Hall magnetoresistance in a canted ferrimagnet. *Phys. Rev. B* **94**, 094401 (2016)
- [26] A. Aqeel, N. Vlietstra, A. Roy, M. Mostovoy, B. J. van Wees, T. T. M. Palstra, Electrical detection of spiral spin structures in Pt|Cu₂OSeO₃ heterostructures. *Phys Rev B.* **94**, 134418 (2016).
- [27] S. H. Baek, S. H. Do, K. Y. Choi, Y. S. Kwon, A. U. B. Wolter, S. Nishimoto, J. van den Brink, B. Büchner, Evidence for a Field-Induced Quantum Spin Liquid in α -RuCl₃. *Phys. Rev. Lett.* **119**, 037201 (2017).
- [28] C. Balz, L. Janssen, P. Lampen-Kelley, A. Banerjee, Y. H. Liu, J. Q. Yan, D. G. Mandrus, M. Vojta, S. E. Nagler, Field-induced intermediate ordered phase and anisotropic interlayer interactions in α -RuCl₃. *Phys. Rev. B* **103**, 174417 (2021).
- [29] K. A. Modic, R. D. McDonald, J. P. C. Ruff, M. D. Bachmann, Y. Lai, J. C. Palmstrom, D. Graf, M. K. Chan, F. F. Balakirev, J. B. Betts, G. S. Boebinger, M. Schmidt, M. J. Lawler, D. A. Sokolov, P. J. W. Moll, B. J. Ramshaw, A. Shekhter, Scale-invariant magnetic anisotropy in RuCl₃ at high magnetic fields. *Nat. Phys.* **17**, 240-244 (2021).
- [30] A. Banerjee, J. Yan, J. Knolle, C. A. Bridges, M. B. Stone, M. D. Lumsden, D. G. Mandrus, D. A. Tennant, R. Moessner, S. E. Nagler, Neutron scattering in the proximate quantum spin liquid α -RuCl₃. *Science* **356**, 1055-1059 (2017).
- [31] C. Eichstaedt, Y. Zhang, P. Laurell, S. Okamoto, A. G. Eguiluz, T. Berlijn, Deriving models for the Kitaev spin-liquid candidate material α -RuCl₃ from first principles. *Phys. Rev. B* **100**, 075110 (2019).
- [32] P. Laurell, S. Okamoto, Dynamical and thermal magnetic properties of the Kitaev spin liquid candidate α -RuCl₃. *npj Quantum Materials* **5**, 2 (2020).
- [33] P. A. Maksimov, A. L. Chernyshev, Rethinking α -RuCl₃. *Phys. Rev. Research* **2**, 033011 (2020).
- [34] J. A. Sears, M. Songvilay, K. W. Plumb, J. P. Clancy, Y. Qiu, Y. Zhao, D. Parshall, Y.-J. Kim, Magnetic order in α -RuCl₃: A honeycomb-lattice quantum magnet with strong spin-orbit coupling. *Phys. Rev. B* **91**, 144420 (2015).
- [35] S. M. Winter, K. Riedl, P. A. Maksimov, A. L. Chernyshev, A. Honecker, R. Valentí, Breakdown of magnons in a strongly spin-orbital coupled magnet. *Nat. Commun.* **8**, 1152 (2017).
- [36] C. Balz, P. Lampen-Kelley, A. Banerjee, J. Yan, Z. Lu, X. Hu, S. M. Yadav, Y. Takano, Y. Liu, D. A. Tennant, M. D. Lumsden, D. Mandrus, S. E. Nagler, Finite field regime for a quantum spin liquid in α -RuCl₃. *Phys. Rev. B.* **100**, 060405(R) (2019).
- [37] H. Suzuki, H. Liu, J. Bertinshaw, K. Ueda, H. Kim, S. Laha, D. Weber, Z. Yang, L. Wang, H. Takahashi, K. Fürsich, M. Minola, B. V. Lotsch, B. J. Kim, H. Yavaş, M. Daghofer, J. Chaloupka, G. Khaliullin, H. Gretarsson, B. Keimer, Proximate ferromagnetic state in the Kitaev model material α -RuCl₃. *Nat. Commun.* **12**, 4512 (2021).
- [38] Y. Nagai, T. Jinno, J. Yoshitake, J. Nasu, Y. Motome, M. Itoh, Y. Shimizu, Two-step gap opening across the quantum critical point in the Kitaev honeycomb magnet α -RuCl₃. *Phys. Rev. B* **101**, 020414 (2020).
- [39] S. Gass, P. M. C onsoli, V. Kocsis, L. T. Corredor, P. Lampen-Kelley, D. G. Mandrus, S. E. Nagler, L. Janssen, M. Vojta, B. B uchner, A. U. B. Wolter, Field-induced transitions in the Kitaev material α -RuCl₃ probed by thermal expansion and magnetostriction. *Phys. Rev. B* **101**, 245158 (2020).
- [40] D. Wulferding, Y. Choi, S.-H. Do, C. H. Lee, P. Lemmens, C. Faugeras, Y. Gallais, K.-Y. Choi, Magnon bound states versus anyonic Majorana excitations in the Kitaev honeycomb magnet α -RuCl₃. *Nat. Commun.* **11**, 1603 (2020).
- [41] Z. Wang, S. Reschke, D. H uvonen, S. H. Do, K. Y. Choi, M. Gensch, U. Nagel, T. R od om, A. Loidl, Magnetic Excitations and Continuum of a Possibly Field-Induced Quantum Spin Liquid in α -RuCl₃. *Phys. Rev. Lett.* **119**, 227202 (2017).

- [42] O. Tanaka, Y. Mizukami, R. Harasawa, K. Hashimoto, K. Hwang, N. Kurita, H. Tanaka, S. Fujimoto, Y. Matsuda, E. G. Moon, T. Shibauchi, Thermodynamic evidence for field-angle dependent Majorana gap in a Kitaev spin liquid. *Nat. Phys.* <https://doi.org/10.1038/s41567-021-01488-6> (2022).
- [43] D. Takikawa, S. Fujimoto, Impact of off-diagonal exchange interactions on the Kitaev spin-liquid state of α -RuCl₃. *Phys. Rev. B* **99**, 224409 (2019).
- [44] D. Hirobe, M. Sato, T. Kawamata, Y. Shiomi, K.-i. Uchida, R. Iguchi, Y. Koike, S. Maekawa, E. Saitoh. One-dimensional spinon spin currents. *Nat. Phys.* **13**, 30-34 (2017).
- [45] G. Jackeli, G. Khaliullin, Mott Insulators in the Strong Spin-Orbit Coupling Limit: From Heisenberg to a Quantum Compass and Kitaev Models. *Phys. Rev. Lett.* **102**, 017205 (2009).
- [46] T. Kato, Y. Ohnuma, M. Matsuo, Microscopic Theory of Spin Hall Magnetoresistance. *Phys. Rev. B* **102**, 094437 (2020).
- [47] A. Sears, L. E. Chern, S. Kim, P. J. Bereciartua, S. Francoual, Y. B. Kim, Y.-J. Kim, Ferromagnetic Kitaev interaction and the origin of large magnetic anisotropy in α -RuCl₃. *Nat. Phys.* **16**, 837-840 (2020).
- [48] L. Janssen, E. C. Andrade, M. Vojta, Magnetization processes of zigzag states on the honeycomb lattice: Identifying spin models for α -RuCl₃ and Na₂IrO₃. *Phys. Rev. B* **96**, 064430 (2017).
- [49] M. Gohlke, G. Wachtel, Y. Yamaji, F. Pollmann, Y. B. Kim. Quantum spin liquid signatures in Kitaev-like frustrated magnets. *Phys. Rev. B* **97**, 075126 (2018).

Figures and Tables

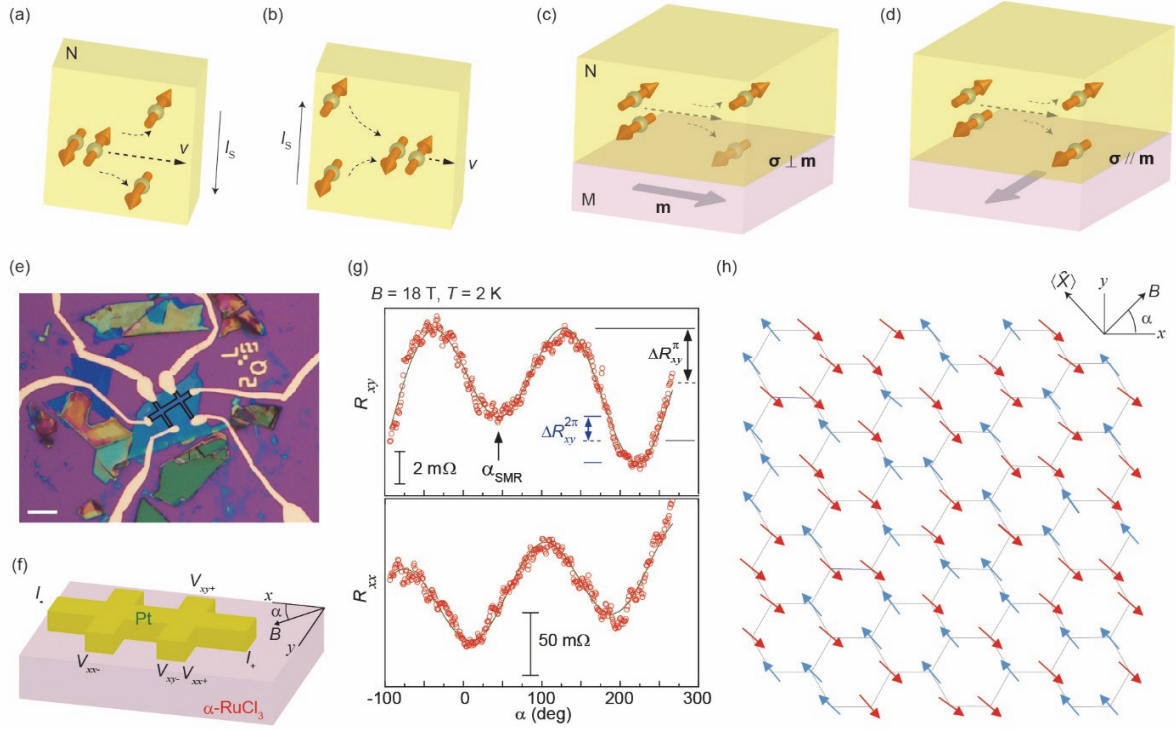


FIG. 1. Spin sensitive transport and spin-Hall magnetoresistance (SMR). (a) Direct spin Hall effect in a nonmagnetic spin-Hall metal N (such as Pt used in our work). The charge current (indicated by velocity v) induces spin accumulation at the surface with spin current I_s . (b) Inverse spin Hall effect converts spin current to electric charge current. (c,d) Spin Hall effect in a magnet(M)/ N bilayer. When current flows in N, the spin Hall effect generates spin polarization (σ) accumulation at the interface. The spin-dependent interaction between σ and the magnetic moment (m) in the magnetic material (M) depends on their relative angle. The different interactions between the transverse (c) and parallel (d) cases causes different efficiencies for spins to be reflected from the interface back to N and converted to charge current. The apparent longitudinal resistivities are therefore different, giving rise to SMR. (e) Optical micrograph of an α -RuCl₃/Pt heterostructure (device #1). Scale bar is 10 μ m. The 3-nm-thick Pt Hall bar is fabricated on the flat surface of a cleaved α -RuCl₃ flake (whose thickness is 50 nm). The black line is to indicate the boundary of the Hall bar. (f) Schematic of device and electrical transport measurement. The in-plane angle α of the magnetic field (B) is defined from the direction (x) of current flow. The SMR causes a $\cos(2\alpha+\pi/2)$ dependence for R_{xy} and $\cos(2\alpha+\pi)$ dependence for R_{xx} if the relevant direction of the magnetic moment in α -RuCl₃ stays perpendicular to and co-rotates with the magnetic field direction (as in AFMs studied in previous SMR measurements). (g) Oscillation of transverse and longitudinal resistances as functions of α measured with the in-plane magnetic field B of 18 T and at $T = 2$ K. $\Delta R_{xy}^{2\pi}$ and ΔR_{xy}^{π} indicate the amplitudes of fitted oscillation components with a period of 2π and π respectively. α_{SMR} denotes the first positive angle position of the local minimum in the R_{xy} oscillation component with the period π . (h) A proposed possible snapshot of local spin (S) configuration relevant for SMR in α -RuCl₃ under external in-plane magnetic field B . The red and blue arrows indicate spins with mostly opposite directions, but slightly tilted towards the B field direction to give a small longitudinal magnetic moment. The quantization axes \hat{X} (see eq.3 and main text) of the spins are mostly perpendicular to the external B field, resulting in $S_x S_y$ (which contributes to SMR [21]) to be always negative.

$\langle \hat{X} \rangle$ indicates spatial average of \hat{X} . In this snapshot, there are equal number of antiferromagnetic and ferromagnetic bonds (two neighboring spins having different or same colors), without any magnetic superlattices. The snapshot also satisfies that $\langle n \rangle \equiv \langle S_A - S_B \rangle = 0$ where S_A and S_B are spins on sublattice A and B, i.e. an antiferromagnetic order is not present.

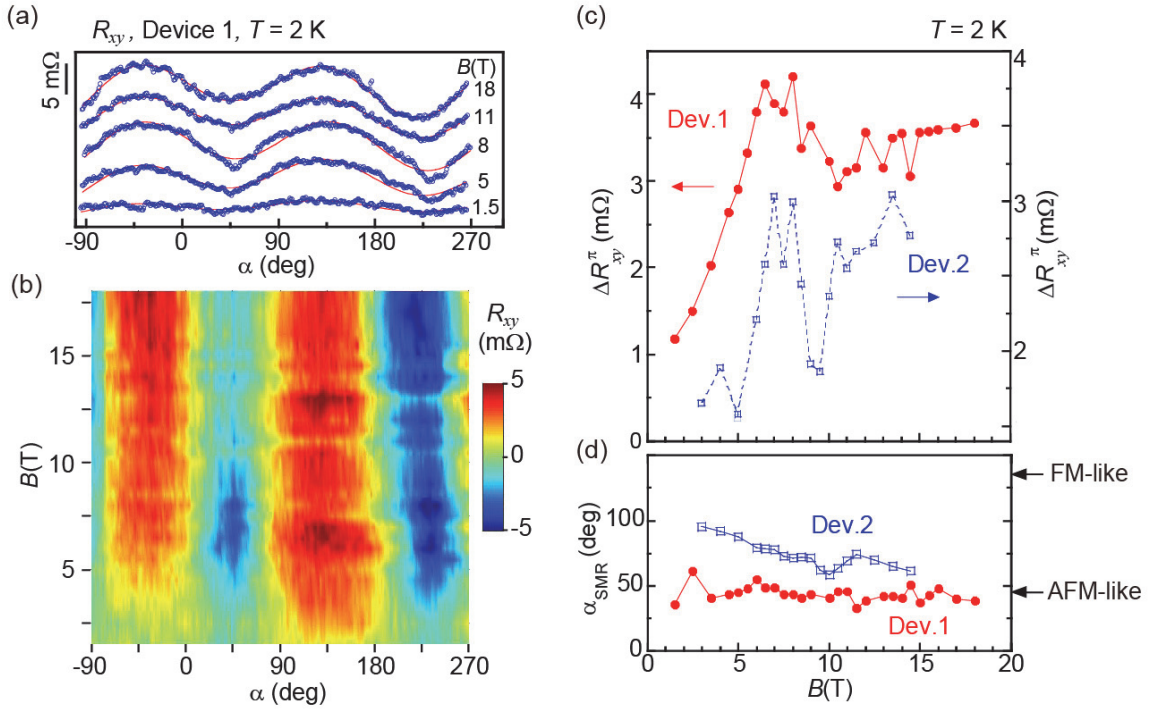


FIG. 2. Magnetic field evolution of the angular oscillation of SMR. (a) The angular oscillation in the Hall resistance (R_{xy}) at $T = 2$ K under representative magnetic fields of 18 T, 11 T, 8 T, 5 T, and 1.5 T. Angular oscillation with a period of π is clearly visible, resulting from the anisotropic longitudinal resistivity (Fig.1). The solid red lines are obtained by fitting (see text for details). The curves are shifted vertically for clarity. The scale bar shows 5 $m\Omega$. (b) The magnetic field (B) evolution of the angle (α)-dependent R_{xy} (with interpolation between traces measured at adjacent B fields) shown in the color (scale bar on the right). A constant background is fitted and subtracted from each trace for the clarity. (c,d) The magnetic field evolution of the amplitude (c) and the phase (d) of the π -periodic oscillation in R_{xy} at $T = 2$ K for the device #1 (red closed circle, labeled as Dev. 1) and the device #2 (blue open rectangle, Dev. 2). For SMR studied so far, $\alpha_{SMR} = 45^\circ$ for antiferromagnets and 135° for ferromagnets (see the main text for details).

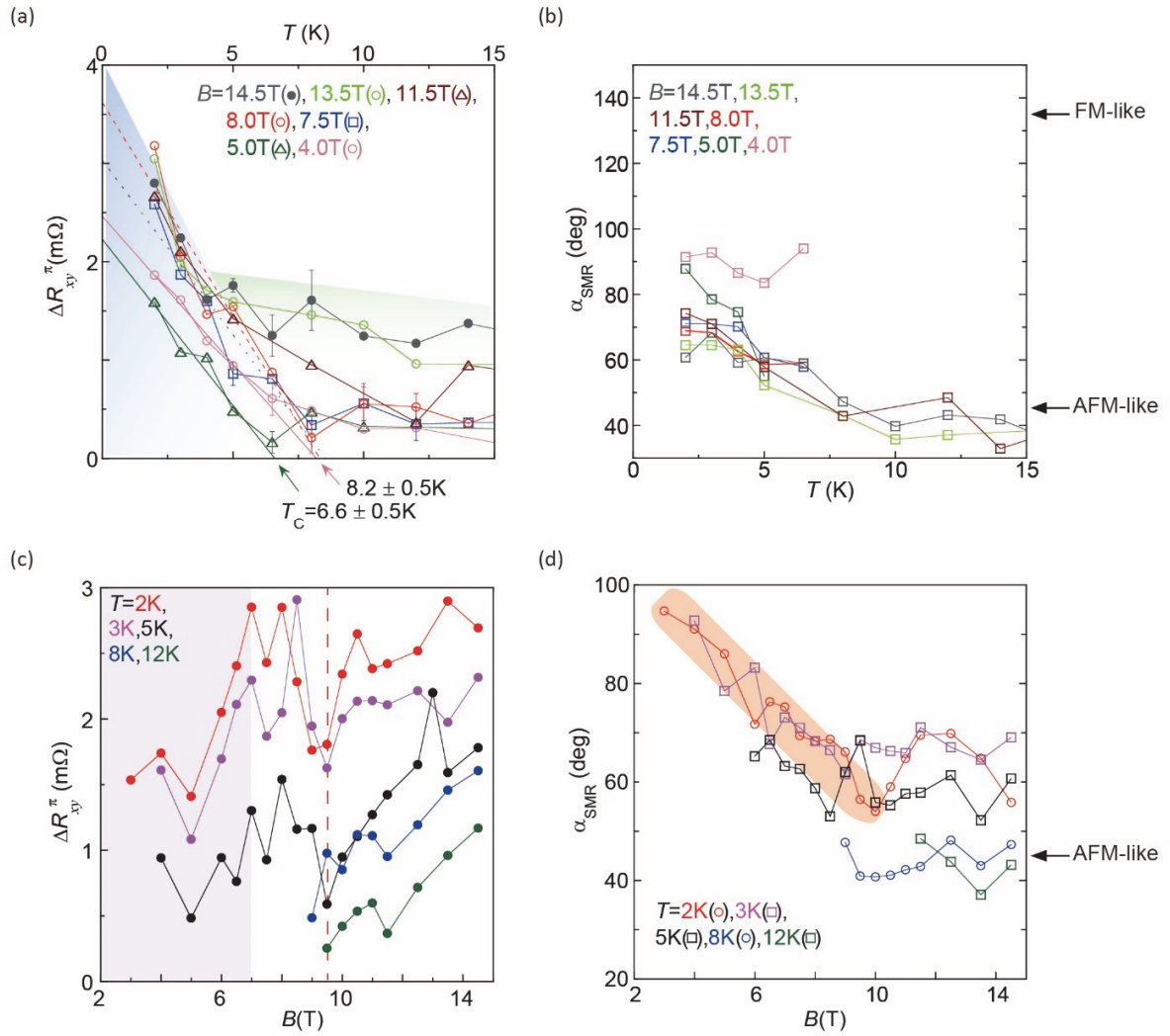


FIG. 3. SMR at elevated temperatures. (a) Temperature evolution of the SMR oscillation amplitude ΔR_{xy}^{π} measured for device #2 under the in-plane fields of 14.5 T (gray), 13.5 T (light green), 11.5 T (brown), 8.0 T (red), 7.5 T (blue), 5.0 T (green), and 4.0 T (pink). At lower B fields, ΔR_{xy}^{π} rapidly decreases with increasing temperature before the signal (angular oscillation of R_{xy}) becomes difficult to discern from the noise level (typically ~ 0.5 m Ω). The linear fits show the intercepts to $\Delta R_{xy}^{\pi} = 0$ at the temperatures of 6.6 K and 8.2 K for $B = 4.0$ T and $B = 5.0$ T, respectively (shown by green and pink arrows), a temperature scale consistent with that of the previously reported phase transition from an antiferromagnet to a paramagnet phase (5,25,32). The behavior is markedly different at the high field of 14.5 T, where the SMR oscillation is clearly observed up to high temperatures. The region for the rapid linear decrease with temperature is marked with shaded blue area. The other region (with slower decrease with temperature) is marked with shaded green area. (b) The temperature evolution of the phase (α_{SMR}) of the SMR oscillation for the same set of magnetic fields in (a). The SMR phase remains antiferromagnetic-like at high temperatures. The expected phases for ferromagnetic (FM)- and antiferromagnetic (AFM)-like SMR oscillation are indicated by arrows. (c) The field evolution of SMR amplitude for the temperature of 2 K (red), 3 K (violet), 5 K (black), 8 K (blue) and 12 K (green). The purple box indicates expected magnetic field range of AFM phase and the red dotted line is shown at $B = 9.5$ T. (d) The field evolution of SMR phase for the same set of temperatures in (c). The region where the phase rapidly changes is highlighted by the shaded orange rectangle.

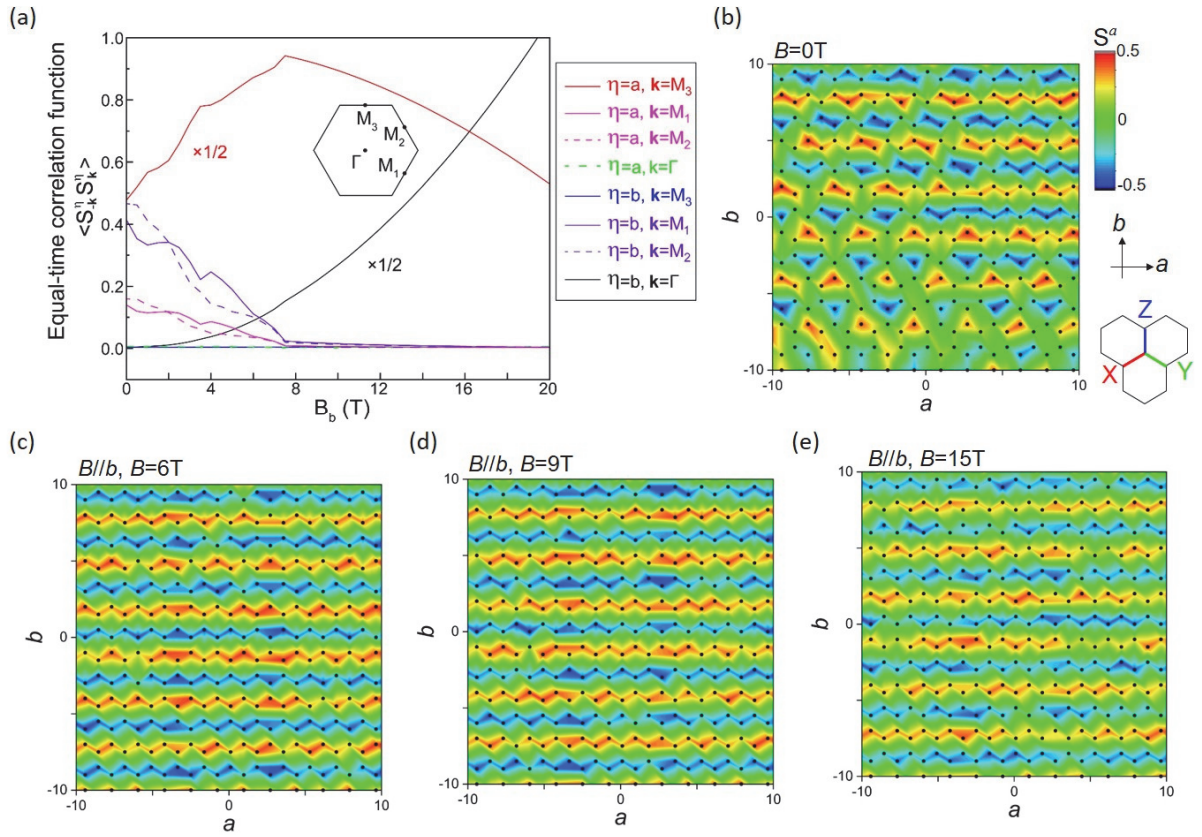


FIG. 4. A simulation of the spin configuration in α -RuCl₃ and evolution with magnetic field. (a) Momentum-dependent spin correlations (“equal-time correlation”) as functions of in-plane magnetic fields calculated by a classical Monte Carlo (MC) simulation performed at $T = 2$ K, based on the parameters $J_1 = -1.3$ meV, $K_1 = -15.1$ meV, $\Gamma_1 = 10.1$ meV, $\Gamma_1' = -0.1175$ meV, $J_3 = 0.9$ meV [30]. Inset shows the first (solid line) and the second (dotted line) Brillouin zones for the honeycomb lattice with the notations for momentum space (magnetic field is along b or ΓM_3 direction, see also Fig.S5). The upper (η) and the lower (\mathbf{k}) indices of the correlation function represent the direction of spin component and the momentum for which the spin correlation are evaluated, and $\langle \dots \rangle$ represents statistical average. The curve for $\eta = a, \mathbf{k} = M_3$, i.e., $\langle S_{-M_3}^a S_{M_3}^a \rangle$, reveals a zigzag antiferromagnetic (AFM) correlation with a minimum period in b direction, significant even at very high field. (b)-(e) Snapshots of real space spin configuration (S^a) calculated by MC method under the in-plane magnetic fields of 0 T, 6 T, 9 T and 15 T, from (b) to (e), respectively. The unit of the a and b axes is the nearest neighbor Ru-Ru bond length. Dots indicate the position of lattice spins. Color shows a spin component (S^a) perpendicular to the field direction (along b). Contour plots were drawn by interpolating the values on hexagonal lattice. Note the simulation cannot reveal whether the snapshots fluctuate or not with time, and thus only reveals AFM correlation rather than AFM order. Inset in (b) shows the axes a and b , and the bonds $X, Y,$ and Z . The field is applied along b direction for (a) to (e).

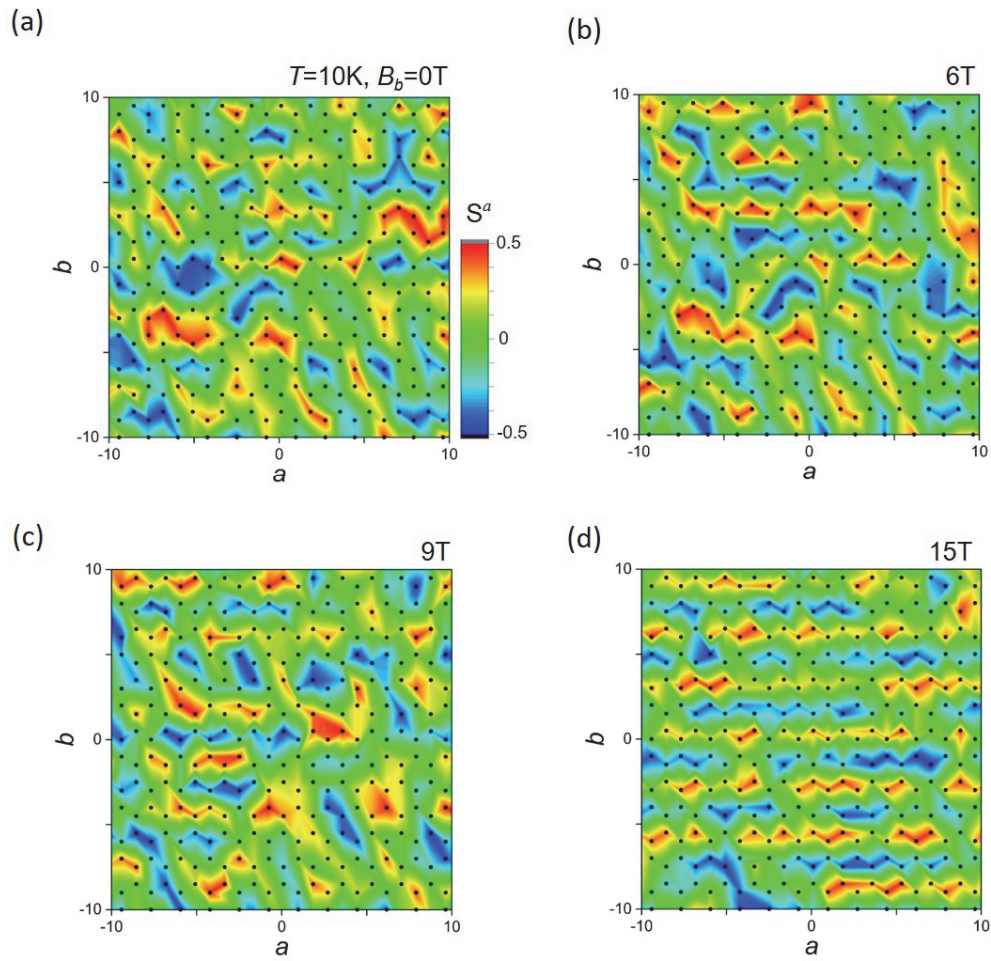


FIG. 5. Spin configurations at elevated temperature computed by a classical Monte Carlo simulation. Real space spin component (S^a) at $T = 10$ K under the in-plane magnetic field (applied along b) of 0 T, 6 T, 9 T and 15 T, from (a) to (d), plotted in the same scheme with Figs.4 (b)-(e). While antiferromagnetic correlation is not noted at 0 T, it appears at the higher field of 15 T.